ChemComm

COMMUNICATION

View Article Online
View Journal

Cite this: DOI: 10.1039/d4cc02207f

Received 7th May 2024,
Accepted 26th June 2024

DOI: 10.1039/d4cc02207f

rsc.li/chemcomm

CO_2 cleavage by tantalum/M (M = iridium, osmium) heterobimetallic complexes†

Abdelhak Lachguar,[a] Christopher Z. Ye,[bc] Sheridon N. Kelly,[bc] Erwann Jeanneau,[d] Iker Del Rosal,[e] Laurent Maron,[e] Laurent Veyre,[a] Chloé Thieuleux,[a] John Arnold *[bc] and Clément Camp *[a]

A novel Ta/Os heterobimetallic complex, $[Ta(CH_2tBu)_3(\mu\text{-}H)_3OsCp^*]$, 2, is prepared by protonolysis of $Ta(CHtBu)(CH_2tBu)_3$ with Cp^*OsH_5. Treatment of 2 and its iridium analogue $[Ta(CH_2tBu)_3(\mu\text{-}H)_2IrCp^*]$, 1, with CO_2 under mild conditions reveal the efficient cleavage of CO_2, driven by the formation of a tantalum oxo species in conjunction with CO transfer to the osmium or iridium fragments, to form $Cp^*Ir(CO)H_2$ and $Cp^*Os(CO)H_3$, respectively. This bimetallic reactivity diverges from more classical CO_2 insertion into metal–X (X = metal, hydride, alkyl) bonds.

The design of synthetic bimetallic complexes associating different metals with complementary Lewis acidic/Lewis basic behaviour has raised interest for cooperative reactivity,[1–10] including CO_2 activation.[11–17] In many instances, these bifunctional complexes lead to CO_2 adducts or insertion products, in which a bent CO_2 fragment binds across the two metals.[18–27] In contrast, only a few heterobimetallic complexes have clearly exhibited the capability to cleave the C–O bond within CO_2. Thomas and colleagues reported oxidative CO_2 cleavage across the early/late heterobimetallic complex $Co(iPr_2PNMes)_3Zr(THF)$, yielding $(OC)Co(iPr_2PNMes)_2(\mu\text{-}O)Zr(iPr_2PNMes)$ at ambient temperature (Scheme 1a).[28] The Mazzanti group reported the potassium-assisted reductive cleavage of CO_2 by a U(III) siloxide complex, resulting in CO evolution and the formation of a pentavalent uranium oxo complex (Scheme 1b). When the potassium cation is encapsulated in 18-crown-6, bimetallic cooperativity no longer occurs, and a carbonate complex is formed instead. Our group has developed an Ir/Al-based heterobimetallic complex proficient in CO_2 deoxygenation, yielding $Cp^*Ir(CO)H_2$, Cp^*IrH_4, and $[Al(Py)(OAr)(iBu)]_2(\mu\text{-}O)$ at room temperature (Scheme 1c).[29] Recently, Campos and coworkers reported the use of $Al(C_6F_5)_3$ for triggering the bimetallic cleavage of Fe-bound CO_2 moiety, to form an oxo carbonyl complex (Scheme 1d). The choice of the Al-based Lewis acid partner plays a pivotal role in initiating this reaction, as boron, zinc, or gold Lewis acids did not exhibit activity in this transformation.[22] Finding right bimetallic combinations therefore remains a major challenge for controlling reactivity.

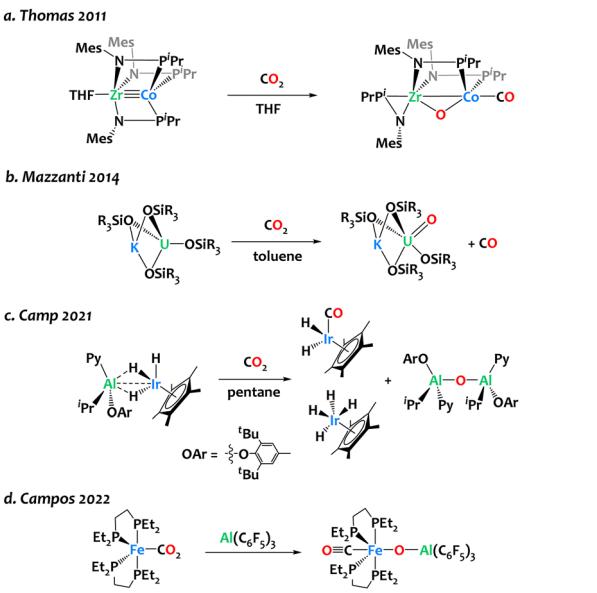

Scheme 1 Reports of CO_2 cleavage by heterobimetallic complexes relevant to the present study.[22,28–30]

[a] Laboratory of Catalysis, Polymerization, Processes and Materials (CP2M UMR 5128) CNRS, Universite Claude Bernard Lyon 1, CPE-Lyon, Institut de Chimie de Lyon, 43 Bvd du 11 Novembre 1918, 69616 Villeurbanne, France. E-mail: clement.camp@univ-lyon1.fr
[b] Department of Chemistry, University of California, Berkeley, California 94720, USA. E-mail: arnold@berkeley.edu
[c] Chemical Sciences Division, Lawrence Berkeley National Laboratory, Berkeley, California 94720, USA
[d] Centre de Diffractométrie Henri Longchambon, Universite Claude Bernard Lyon 1, 5 Rue de la Doua, 69100 Villeurbanne, France
[e] Université de Toulouse, CNRS, INSA, UPS, UMR5215, LCPNO, 135 Avenue de Rangueil, F-31077 Toulouse, France

† Electronic supplementary information (ESI) available: Experimental procedure and additional characterization data. CCDC 2351192 and 2351850. For ESI and crystallographic data in CIF or other electronic format see DOI: https://doi.org/10.1039/d4cc02207f

The alkane elimination reaction between metal (poly)alkyls and (poly)hydride species has proven efficient for accessing heterobimetallic complexes.[31–36] We used this strategy to synthesize compound [Ta(CH_2tBu)$_3$IrH_2Cp*] **1** from the tantalum tris-neopentyl neopentylidene complex Ta(C*H*tBu)(CH_2tBu)$_3$ and the iridium tetrahydride complex Cp*IrH_4 (Scheme 2-top).[37] This prompted us to extend this chemistry by investigating the reactivity of Ta(C*H*tBu)(CH_2tBu)$_3$ towards related 6d metal polyhydrides. Treating Ta(C*H*tBu)(CH_2tBu)$_3$ with Cp*OsH_5[38,39] in a 1 : 1 stoichiometric ratio in pentane at room temperature yields the heterobimetallic complex [Ta(CH_2tBu)$_3$(μ-H)$_3$OsCp*] **2** in 98% isolated yield, accompanied by the elimination of one equivalent of neopentane (Scheme 2-middle). ^{1}H NMR monitoring of the reaction of **2** with Cp*OsH_5 (1 equiv.) suggests the slow formation of a trinuclear $TaOs_2$ species (see Fig. S7, ESI†), analogous to the $TaIr_2$ species previously reported.[40] Surprisingly, Cp*ReH_6[41] shows no reactivity towards Ta(C*H*tBu)(CH_2tBu)$_3$ either in pentane at room temperature or in C_6D_6 at 80 °C. DFT calculations indicate that the Ta/Re analogue should be thermodynamically stable: this observed lack of reactivity is thus surprising, and might be due to the lack of available coordination site at Re (see ESI† for discussion).

Identification of **2** is confirmed through a range of analytical methods including infrared (IR) and multinuclei (^{1}H, ^{13}C, ^{1}H–^{1}H COSY, ^{1}H–^{13}C HSQC and HMBC) solution NMR spectroscopy, elemental analysis, and X-ray diffraction studies. In the ^{1}H-NMR spectrum of **2** obtained in a toluene-d_8 solution, the hydride resonance appears as a high-field singlet at δ = −6.90 ppm, integrating for 3H. The hydride resonance in **2** exhibits a shift of $\Delta\delta$ = +4.3 ppm from Cp*OsH_5 which is reminiscent of the observed shift from Cp*IrCH_4 to **1**, of approximately $\Delta\delta$ = +3.5 ppm.[37] The IR spectrum of compound **2** displays a characteristic metal-hydride stretching vibration signal at 1961 cm^{-1}, consistent with bridging hydrides. This value deviates significantly from that of complex [Ta(CH_2tBu)$_3$IrCp*(H)$_2$], **1**, featuring two terminal hydrides (ν_{Ir-H} = 2061 cm^{-1}, see Fig. S6, ESI†) and that of the Cp*OsH_5 precursor, which exhibits a strong absorption at 2083 (s) cm^{-1} with a minor one at 2214 (w) cm^{-1}.[42] For comparison, the metal-hydride stretch is observed at 1982 cm^{-1} in [Hf(CH_2tBu)$_3$(μ-H)$_3$IrCp*][34] and at 1952 and 1970 cm^{-1} for [Cp_2Zr(X)(μ-H)$_3$Os(PMe_2Ph)$_3$] (X = Cl or H respectively),[43] where the two metal centres are bridged by three hydride ligands.

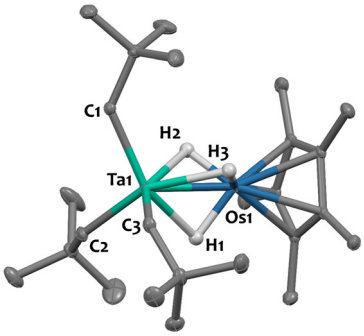

Fig. 1 Solid-state molecular structure of **2** (30% probability ellipsoids). Hydrogen atoms from the hydrocarbon ligands are omitted for clarity. Selected bond distances (Å) and angles (°): Ta1–Os1 2.4817(2), Ta1–C1 2.132(3), Ta1–C2 2.136(3), Ta1–C3 2.143(3), Os1–H1 1.45(5), Os1–H2 1.56(5), Os1–H3 1.48(8), Ta1–H1 2.07(5), Ta1–H2 2.03(5), Ta1–H3 2.07(8), Ta1–Os1–Cp*$_{centroid}$ 178.1(1).

Single crystals of **2** suitable for X-ray diffraction were grown from a saturated pentane solution at −40 °C. The solid-state structure is depicted in Fig. 1. The nearly linear Ta–Os–Cp*$_{centroid}$ angle (178.1(1)°), indicates the presence of three bridging hydrides between the two metals, arranged in a tripod geometry around the {Cp*Os} core. This angle aligns well with values reported for systems featuring similar bridging hydride motifs, such as [CpRu(μ-H)$_4$OsCp*] (179.2(9)°)[44] and [Hf(CH_2tBu)$_3$(μ-H)$_3$IrCp*] (179.2(3)°),[34] but starkly contrasts with that found in complex **1**, featuring two terminal Ir–H moieties (151.3(1)°). The Ta–C_{Np} bond lengths (with an average value of 2.137(5) Å) are consistent with neopentyl groups.[45–47] The Ta–Os distance in compound **2** is 2.4817(2) Å, which is 0.115 Å shorter than the sum of the metallic radii of tantalum (1.343 Å) and osmium (1.255 Å).[48] This difference results in a formal shortness ratio (FSR) slightly below unity (FSR = 0.95),[49] suggestive of some degree of metal–metal interaction, although the presence of bridging hydrides could also explain the proximity. This FSR value lies between those of complex [Hf(CH_2tBu)$_3$(μ-H)$_3$IrCp*] (FSR = 0.99),[34] where the close proximity between the Hf and Ir centres likely results from bridging hydrides, and the Ta/Ir complex **1** (FSR = 0.90),[37] which exhibits clear double metal–metal bonding.

To explore the potential of these heterobimetallic complexes in promoting cooperative reactivity, we investigated the reaction of **1** and **2** with CO_2 (1 atm, *ca.* 6 equiv.). The reactions were carried out in tetrahydrofuran (THF) at ambient temperature, resulting in rapid discoloration of the reaction mixture within *ca.* 10 minutes in both cases. Analysis of the crude reaction mixtures by ^{1}H NMR reveals the complete consumption of complexes **1** and **2**, with clean and quantitative formation of compounds Cp*Os(CO)H_3 **3** and Cp*Ir(CO)H_2 **4**, respectively derived from complexes **1** and **2**, alongside the generation of a tantalum oxo complex, [Ta(O)(CH_2tBu)$_3$]$_x$ **5** (refer to Fig. S9 and S10 in the ESI†).

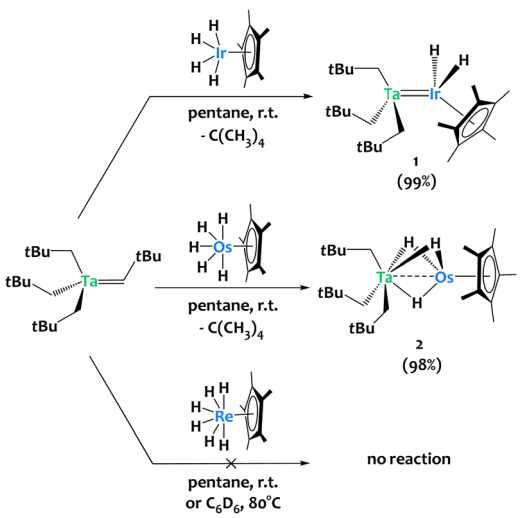

Scheme 2 Reactivity of Ta(C*H*tBu)(CH_2tBu)$_3$ towards Cp*IrH_4, Cp*OsH_5 and Cp*ReH_6.

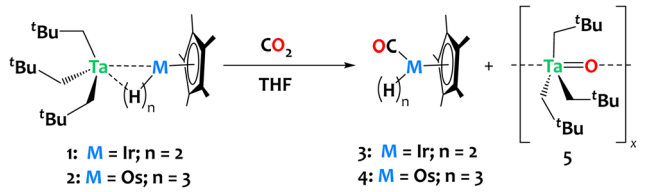

Scheme 3 Reaction of compounds **1** and **2** with CO_2, yielding Cp*Ir(CO)H_2 and Cp*Os(CO)H_3, respectively, together with the formation of Ta(O)(CH_2tBu)$_3$, **5**.

The insolubility of compound **5** in pentane facilitated its separation from the reaction mixtures by simple evaporation of THF followed by pentane extraction of **3** or **4**. Compound **3** was isolated in 96% yield; ^{1}H and ^{13}C NMR data are in agreement with the literature (Scheme 3).[29,50]

The ^{1}H-NMR spectrum of **4**, recorded in THF-d_8, indicates that the three hydrides are not equivalent in solution, resulting in two signals at −10.48 ppm and −12.50 ppm integrating for 1H and 2H, respectively and coupling in the ^{1}H–^{1}H COSY NMR spectrum (Fig. S15, ESI†). These signals are assigned to hydrides in *-trans* and *-cis* positions relative to the CO group, respectively, which is consistent with literature data.[51] The IR spectrum for **4** displays a broad terminal hydride stretching signal at 2075 cm^{-1}, and ν_{CO} bands at 1932–1898 cm^{-1}, as expected.[51] Diluted THF solutions of complex **4** are stable at room temperature in the dark. Yet compound **4** is reported to be unstable in the solid-state,[51] spontaneously eliminating H_2 upon drying, which could explain the moderate 45% isolated yield. Regardless, single crystals suitable for X-ray diffraction were obtained by avoiding visible light and crystallisation from pentane at −40 °C. The solid-state structure of **4**, determined for the first time in this study, is shown in Fig. 2. The Os1–C1 (1.851(3) Å) and O1–C1 (1.162(4) Å) distances are consistent with those observed in compound [Cp*Os(CO)(μ-H)]$_2$, featuring Os–C bond lengths of 1.833(9) Å and C–O bond lengths of 1.18(1) Å.[29]

The ^{1}H-NMR spectrum of **5** indicates that the three CH_2tBu groups are equivalent in solution, resulting in two signals at 0.55 ppm and 1.12 ppm for the CH_2 and *t*Bu moieties, respectively. Analysis of the ^{13}C{^{1}H}-NMR spectrum of **5** reveals three distinct characteristic resonances at 104.3, 35.1 and 34.4 ppm assigned to the $TaCH_2$, $C(CH_3)_3$ and $C(CH_3)_3$ moieties, respectively. These assignments are confirmed by the 2D ^{1}H–^{1}H COSY and ^{1}H–^{13}C HSQC and HMBC data (Fig. S19–S21, ESI†). Unfortunately, we were unable to determine the XRD structure of **5**, which probably adopts oligomeric structures, given that terminal Ta-oxo species are rare in the literature.[52–54] To confirm the identity of **5**, we thus carried out a high resolution mass spectrometry analysis using an APCI source, which shows a clear signal for the ion [Ta(O)(CH_2tBu)$_3$ + H]$^+$ at 411.2086 *m*/*z* (see Fig. S22, ESI†).

The computed reaction mechanism (DFT, B3PW91) is similar for **1** and **2**. CO_2 undergoes first a kinetically accessible (13 kcal mol^{-1} for **1**, 11 kcal mol^{-1} for **2**) nucleophilic attack by the Ir (or Os) center, which is assisted by oxygen-coordination to Ta. This results in 4-member metallacyclic intermediates shown on Fig. 3. The next step is a C–O bond breaking TS (barrier of 9 kcal mol^{-1} for **1** and 14 kcal mol^{-1} for **2**) to yield to products **3** (or **4**) and **5**, which formation is strongly exothermic (see ESI† for reaction profiles).

In summary, the reaction between Cp*OsH_5 and Ta(CH*t*Bu)(CH_2tBu)$_3$ affords a heterobimetallic Ta–Os complex, **2**, in high yields *via* alkane elimination. Complex **2**, along with its Ta–Ir analogue, **1**, exhibit clean CO_2 cleavage reactivity, driven by the formation of a tantalum oxo species in conjunction with late metal carbonyls. Given the propensity of related transition metal alkyls and hydrides for CO_2 insertion,[55–59] the selective, divergent bimetallic reactivity observed herein is notable. These results clearly further demonstrate how the synergistic action of early/late metal assemblies – particularly those based on tantalum – can facilitate the deoxygenation of CO_2. This understanding contributes to advancing knowledge in CO_2 activation and could lead to future applications in deoxygenative chemistry.

This work was funded by the European Union (ERC, DUO, 101041762) and the Director, Office of Science, Office of Basic Energy Sciences, Division of Chemical Sciences, Geosciences, and Biosciences Heavy Element Chemistry Program of the U. S. Department of Energy (DOE) at LBNL under contract DE-AC02-05CH11231. Views and opinions expressed are however those of the authors only and do not necessarily reflect those of the European Union or the European Research Council. Neither the European Union nor the granting authority can be held responsible for them. The authors acknowledge the HPCs CALcul en

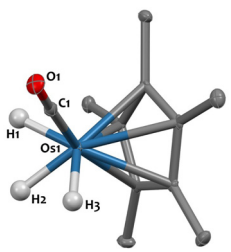

Fig. 2 Solid-state molecular structure of **4** (30% probability ellipsoids). Hydrogen atoms from the Cp* ligand are omitted for clarity. Selected bond distances (Å) and angles (°): Os1–H1 1.53(4), Os1–H2 1.58(4), Os1–H3 1.51(4), Os1–C1 1.851(3), O1–C1 1.162(4), Os1–Cp*$_{centroid}$ 1.916(1), C1–Os1–Cp*$_{centroid}$ 132.5(1).

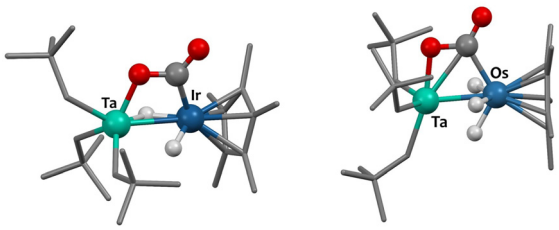

Fig. 3 Computed (DFT) structures of the metallacyclic reaction intermediates.

Midi-Pyrenees (CALMIP-EOS grant 0833). LM is a senior member of the Institut Universitaire de France.

Data availability

The data supporting this article have been included as part of the ESI.† CCDC 2351192 and 2351850 contain supplementary crystallographic data for this article; they can be obtained free of charge from The Cambridge Crystallographic Data Centre.

Conflicts of interest

There are no conflicts to declare.

References

1 P. Buchwalter, J. Rosé and P. Braunstein, *Chem. Rev.*, 2015, **115**, 28–126.
2 E. K. Van Den Beuken and B. L. Feringa, *Tetrahedron*, 1998, **54**, 12985–13011.
3 J. A. Mata, F. E. Hahn and E. Peris, *Chem. Sci.*, 2014, **5**, 1723–1732.
4 A. Lachguar, A. V. Pichugov, T. Neumann, Z. Dubrawski and C. Camp, *Dalt. Trans.*, 2023, **53**, 1393–1409.
5 J. Campos, *Nat. Rev. Chem.*, 2020, **4**, 696–702.
6 N. P. Mankad, *Chem. Commun.*, 2018, **54**, 1291–1302.
7 B. G. Cooper, J. W. Napoline and C. M. Thomas, *Catal. Rev.*, 2012, **54**, 1–40.
8 B. Chatterjee, W. C. Chang, S. Jena and C. Werlé, *ACS Catal.*, 2020, **10**, 14024–14055.
9 T. S. Hollingsworth, R. L. Hollingsworth, R. L. Lord and S. Groysman, *Dalt. Trans.*, 2018, **47**, 10017–10024.
10 C. Z. Ye, I. Del Rosal, S. N. Kelly, I. J. Brackbill, L. Maron, C. Camp and J. Arnold, *Chem. Sci.*, 2024, **15**, 9784–9792.
11 C. Zhang, P. Gotico, R. Guillot, D. Dragoe, W. Leibl, Z. Halime and A. Aukauloo, *Angew. Chem., Int. Ed.*, 2023, **62**, e202214665.
12 D. Ghosh, S. Sinhababu, B. D. Santarsiero and N. P. Mankad, *J. Am. Chem. Soc.*, 2020, **142**, 12635–12642.
13 M. Pérez-Jiménez, H. Corona, F. de la Cruz-Martínez and J. Campos, *Chem. – A Eur. J.*, 2023, **29**, e202301428.
14 Z. B. G. Fickenscher, P. Lönnecke, A. K. Müller, O. Hollóczki, B. Kirchner and E. Hey-Hawkins, *Molecules*, 2023, **28**, 2574.
15 J. Ye, R. C. Cammarota, J. Xie, M. V. Vollmer, D. G. Truhlar, C. J. Cramer, C. C. Lu and L. Gagliardi, *ACS Catal.*, 2018, **8**, 4955–4968.
16 J. R. Prat, C. A. Gaggioli, R. C. Cammarota, E. Bill, L. Gagliardi and C. C. Lu, *Inorg. Chem.*, 2020, **59**, 14251–14262.
17 A. Lachguar, I. Del Rosal, L. Maron, E. Jeanneau, L. Veyre, C. Thieuleux and C. Camp, *J. Am. Chem. Soc.*, 2024, DOI: **10.1021/jacs.4c02172**.
18 S. Sinhababu, M. R. Radzhabov, J. Telser and N. P. Mankad, *J. Am. Chem. Soc.*, 2022, **144**, 3210–3221.
19 J. Hicks, A. Mansikkamäki, P. Vasko, J. M. Goicoechea and S. Aldridge, *Nat. Chem.*, 2019, **11**, 237–241.
20 M. Devillard, R. Declercq, E. Nicolas, A. W. Ehlers, J. Backs, N. Saffon-Merceron, G. Bouhadir, J. C. Slootweg, W. Uhl and D. Bourissou, *J. Am. Chem. Soc.*, 2016, **138**, 4917–4926.
21 G. Fachinetti, C. Floriani and P. F. Zanazzi, *J. Am. Chem. Soc.*, 1978, **100**, 7405–7407.
22 H. Corona, M. Pérez-Jiménez, F. de la Cruz-Martínez, I. Fernández and J. Campos, *Angew. Chem., Int. Ed.*, 2022, **61**, e202207581.
23 C. Yoo and Y. Lee, *Chem. Sci.*, 2016, **8**, 600–605.
24 E. G. Lundquist, J. C. Huffman and K. G. Caulton, *J. Am. Chem. Soc.*, 1986, **108**, 8309–8310.
25 T. A. Hanna, A. M. Baranger and R. G. Bergman, *J. Am. Chem. Soc.*, 1995, **117**, 11363–11364.
26 J. R. Pinkes, B. D. Steffey, J. C. Vites and A. R. Cutler, *Organometallics*, 1994, **13**, 21–23.
27 N. J. Hartmann, G. Wu and T. W. Hayton, *Chem. Sci.*, 2018, **9**, 6580–6588.
28 J. P. Krogman, B. M. Foxman and C. M. Thomas, *J. Am. Chem. Soc.*, 2011, **133**, 14582–14585.
29 L. Escomel, I. Del Rosal, L. Maron, E. Jeanneau, L. Veyre, C. Thieuleux and C. Camp, *J. Am. Chem. Soc.*, 2021, **143**, 4844–4856.
30 O. Cooper, C. Camp, J. Pécaut, C. E. Kefalidis, L. Maron, S. Gambarelli and M. Mazzanti, *J. Am. Chem. Soc.*, 2014, **136**, 6716–6723.
31 M. V. Butovskii, C. Döring, V. Bezugly, F. R. Wagner, Y. Grin and R. Kempe, *Nat. Chem.*, 2010, **2**, 741–744.
32 C. J. Isaac, F. M. Miloserdov, A. F. Pécharman, J. P. Lowe, C. L. McMullin and M. K. Whittlesey, *Organometallics*, 2022, **41**, 2716–2730.
33 L. Escomel, E. Jeanneau, C. Thieuleux and C. Camp, *Inorganics*, 2024, **12**, 72.
34 S. Lassalle, J. Petit, R. L. Falconer, V. Hérault, E. Jeanneau, C. Thieuleux and C. Camp, *Organometallics*, 2022, **41**, 1675–1687.
35 C. Z. Ye, I. Del Rosal, M. A. Boreen, E. T. Ouellette, D. R. Russo, L. Maron, J. Arnold and C. Camp, *Chem. Sci.*, 2022, **14**, 861–868.
36 L. Escomel, N. Soulé, E. Robin, I. Del Rosal, L. Maron, E. Jeanneau, C. Thieuleux and C. Camp, *Inorg. Chem.*, 2022, **61**, 5715–5730.
37 S. Lassalle, R. Jabbour, P. Schiltz, P. Berruyer, T. K. Todorova, L. Veyre, D. Gajan, A. Lesage, C. Thieuleux and C. Camp, *J. Am. Chem. Soc.*, 2019, **141**, 19321–19335.
38 C. L. Gross and G. S. Girolami, *Organometallics*, 2007, **26**, 160–166.
39 C. L. Gross, S. R. Wilson and G. S. Girolami, *J. Am. Chem. Soc.*, 1994, **116**, 10294–10295.
40 S. Lassalle, R. Jabbour, I. Del Rosal, L. Maron, E. Fonda, L. Veyre, D. Gajan, A. Lesage, C. Thieuleux and C. Camp, *J. Catal.*, 2020, **392**, 287–301.
41 W. A. Herrmann, H. G. Theiler, P. Kiprof, J. Tremmel and R. Blom, *J. Organomet. Chem.*, 1990, **395**, 69–84.
42 C. L. Gross and G. S. Girolami, *Organometallics*, 2007, **26**, 160–166.
43 J. W. Bruno, J. C. Huffman, M. A. Green and K. G. Caulton, *J. Am. Chem. Soc.*, 1984, **106**, 8310–8312.
44 T. Shima and H. Suzuki, *Organometallics*, 2005, **24**, 3939–3945.
45 L. J. Guggenberger and R. R. Schrock, *J. Am. Chem. Soc.*, 1975, **97**, 2935.
46 R. Srivastava, E. A. Quadrelli and C. Camp, *Dalt. Trans.*, 2020, **49**, 3120–3128.
47 R. Srivastava, R. Moneuse, J. Petit, P.-A. A. Pavard, V. Dardun, M. Rivat, P. Schiltz, M. Solari, E. Jeanneau, L. Veyre, C. Thieuleux, E. A. Quadrelli and C. Camp, *Chem. – Eur. J.*, 2018, **24**, 4361–4370.
48 L. Pauling, *J. Am. Chem. Soc.*, 1947, **69**, 542–553.
49 F. A. Cotton, *Acc. Chem. Res.*, 1978, **11**, 225–232.
50 D. M. Heinekey, D. A. Fine, T. G. P. Harper and S. T. Michel, *Can. J. Chem.*, 1995, **73**, 1116–1125.
51 J. K. Hoyano and W. A. G. Graham, *J. Am. Chem. Soc.*, 1982, **104**, 3722–3723.
52 J. I. Fostvedt, M. A. Boreen, R. G. Bergman and J. Arnold, *Inorg. Chem.*, 2021, **60**, 9912–9931.
53 S. M. Mullins, R. G. Bergman and J. Arnold, *Organometallics*, 1999, **18**, 4465–4467.
54 P. Horrillo-Martinez, B. O. Patrick, L. L. Schafer and M. D. Fryzuk, *Dalt. Trans.*, 2012, **41**, 1609–1616.
55 M. K. Whittlesey, R. N. Perutz and M. H. Moore, *Organometallics*, 1996, **15**, 5166–5169.
56 O. R. Allen, S. J. Dalgarno, L. D. Field, P. Jensen, A. J. Turnbull and A. C. Willis, *Organometallics*, 2008, **27**, 2092–2098.
57 J. Sánchez-Nieves and P. Royo, *J. Organomet. Chem.*, 2001, **621**, 299–303.
58 M. A. Rankin and C. C. Cummins, *J. Am. Chem. Soc.*, 2010, **132**, 10021–10023.
59 J. M. Mörsdorf and J. Ballmann, *Inorg. Chem.*, 2021, **60**, 18291–18295.